doi:10.26443/seismica.v5i2.1770

Enhanced View of the M_w 6.4 Petrinja (Croatia) Earthquake Sequence (2020–2022) Using Deep Learning

Dinko Šindija * † [1], **Marija Mustać Brčić** [1], **György Hetényi** [2], **Josip Stipčević** [1]

[1]Department of Geophysics, University of Zagreb, Zagreb, Croatia, [2]Institute of Earth Sciences, University of Lausanne, Lausanne, Switzerland

Author contributions: *Methodology*: DS. *Formal Analysis*: DS. *Resources*: MMB, JS. *Writing - Original draft*: DS. *Writing - Review & Editing*: JS, GH, DS. *Visualization*: DS.

Abstract Machine learning approaches have shown potential to automate the creation of seismic catalogues, but their abilities and performance are still questioned and being tested. We here present the Petrinja Earthquake Sequence Machine Learning Catalogue (PESMLC), generated using the EQTransformer seismic phase picker trained on the INSTANCE dataset, PyOcto for phase association, and NonLinLoc for event relocation. Our study focuses on the 2020 M_w 6.4 Petrinja earthquake sequence in Croatia, covering the period from 28 December 2020 to 30 November 2022, during which we detected 41,989 seismic events. PESMLC achieves high matching rates — 96% for the first six months, and 85% over the complete study duration — when compared with detailed manual catalogues. The seismic network densification in January 2021 significantly enhanced event detection reliability, highlighting the importance of network configuration in efficient seismic monitoring. While our machine learning approach successfully identified previously undetected microseismicity and dramatically reduced processing time, we observed systematic limitations, including magnitude estimation biases and difficulties in accurately distinguishing closely spaced events in time. Optimisation of associator parameters remains essential, and should ideally be performed specifically for each network configuration, particularly for fully automated seismic monitoring systems. We further demonstrate that raw machine learning catalogues require quality filtering prior to seismological analysis: stricter magnitude of completeness estimators result in artificially high thresholds for unfiltered machine learning catalogues, and Omori p exponents are biased downward by low-quality detections. Both effects are resolved when analysis is restricted to a quality-filtered subset, which recovers parameters consistent with high-quality manual catalogues. Nevertheless, PESMLC overall provides a detailed, comprehensive seismic dataset aligned closely with manual catalogues, demonstrating the considerable potential of machine learning to support routine seismic monitoring, particularly in resource-limited observatories and/or for long seismic sequences and large datasets.

Production Editor:
Andrea Llenos
Handling Editor:
Robert Skoumal
Copy & Layout Editor:
Tara Nye

Received:
June 23, 2025
Accepted:
August 18, 2026
Published:
September 18, 2026

1 Introduction

Over the last decade, the seismology community saw an accelerating growth in the volume of obtained seismic data driven by the deployment of numerous new seismic stations, arrays, and networks. This vast amount of seismic data necessitates the implementation of automated algorithms to efficiently process earthquake sequence recordings. The traditional method, reliant on manual inspection and labelling of obtained waveforms, is grinding and, crucially, time consuming, especially in the case of dense seismic networks, long seismic sequences, and smaller, underfunded institutions. In recent years, machine learning (ML) has emerged as a promising and widely used alternative for seismic detection and phase picking. ML algorithms, particularly convolutional neural networks (CNN), have demonstrated an ability to automatically detect and classify seismic phases (e.g., P wave, S wave) with high accuracy often comparable to manual picking performance (e.g. Ross et al., 2018, 2019; Zhu and Beroza, 2018; Mousavi et al., 2020). These neural network model approaches can process large volumes of continuous seismic data and adapt to various noise conditions, making them particularly useful for detecting low-magnitude events resulting in more complete earthquake catalogues (Tan et al., 2021). In contrast, traditional automated approaches to earthquake phase-picking, such as the amplitude-based short-term average to long-term average (STA/LTA) method (Allen, 1978), are unreliable in low signal-to-noise ratio (SNR) environments. Existing semi-automatic event detection approaches designed to detect smaller events, such as template matching, require signals of interest to be identified a priori, meaning that earthquakes with waveforms dissimilar to any template will likely remain undetected. On the other hand, ML models can generalise across various seismic networks with little to no manual adjustment, provided that they are trained on representative datasets. This is particularly advantageous when ex-

*Corresponding author: d.sindija@uea.ac.uk
†Now at the University of East Anglia, United Kingdom

panding or modifying a seismic network, as the models can continue to function effectively even with newly deployed stations. Studies have explored application of ML methods in different geographic regions (e.g. China (Jiang et al., 2021); New Zealand (Pita-Sllim et al., 2023); Chile (Woollam et al., 2019); and Italy (Tan et al., 2021)), in volcanic settings (e.g. Suarez et al., 2023; Kim et al., 2022), by using ocean bottom seismometers (Niksejel and Zhang, 2024), and even for studying deep Earth (Zhou et al., 2024).

ML methods are often employed as 'black-boxes', but it is crucial to understand precisely what these models detect, how they reach their decisions, and how they compare with the manual approach (Majstorović et al., 2022). In this study, by comparing with two detailed, manually obtained seismic catalogues, we explore how accurate ML-based methods are. We focus on the 2020 M_w 6.4 Petrinja earthquake sequence in Croatia, a still ongoing seismic sequence, during which the seismic network underwent several changes. By analysing the performance of the ML approach, this study aims to evaluate the accuracy, limitations, and advantages of ML-based seismic detection methods in comparison with manual approaches, and to provide insights into how seismic network configuration influences their reliability.

2 Case study - Petrinja earthquake sequence

2.1 Tectonic setting

The 2020 M_w 6.4 Petrinja earthquake (Herak and Herak, 2023) occurred in central Croatia (Figure 1). The Petrinja earthquake sequence started on 28 December 2020, with a M_w 4.9 foreshock at 05:28 UTC. The following morning, on 29 December at 11:19 UTC, the devastating M_w 6.4 mainshock occurred causing great damage in the greater epicentral area, and was strongly felt throughout Croatia, in the neighbouring countries Slovenia, Bosnia and Herzegovina, Serbia, and Hungary, and in parts of Italy and Austria. The epicentre of the earthquake was located approximately 6 km southwest of the town of Petrinja and about 48 km south-southeast of Zagreb, the nation's capital. The causative fault was identified as the Petrinja fault, a right-lateral strike-slip fault, which lies within the broader Kupa Valley Fault Zone. This fault zone has been seismically active in the past, including the significant 1909 Kupa Valley earthquake, which played a key role in the discovery of the Mohorovičić discontinuity (Mohorovičić, 1910, 1992; Herak and Herak, 2010). The region is located at the contact between the Internal Dinarides and the Pannonian Basin, which leads to a complex tectonic environment. Prior to this earthquake sequence, the European Database of Seismogenic Faults (EDSF, Basili et al., 2013) described this fault zone as transpressional composite source with general fault dip towards NE. This was later updated in the European Fault-Source Model 2020 (EFSM20, Basili et al., 2020) to be classified as right-lateral fault with the same geometry. Herak (2025) calculated fault-plane solutions (FPS) and showed that seismic sources in the Kupa Valley Fault Zone have a Dinaric strike (SE-NW). Both foreshock and mainshock of this sequence exhibit pure lateral strike-slip motion (Figure 1) on a subvertical Petrinja fault which was activated in the length of 20 km (Herak and Herak, 2023). Although most of the seismicity showed strike-slip FPS, Herak (2025) finds some smaller events with reverse faulting. This complements the EFSM20 model which classifies Kupa Valley fault as right lateral strike-slip, with expected dip between 55° and 70°, and rake between 120° and 170°, meaning significant reverse motion is also plausible. Further, for this earthquake sequence, Herak and Herak (2023) locate the depth of seismic activity in the region ranging from 7 to 18 km. As this is an area with a high geothermal gradient, Herak and Herak (2023) suggest that the presence of ophiolite-dominated crust may have allowed brittle deformation at higher-than-usual temperatures where deeper aftershocks were estimated.

Seismological data that were mainly used in Petrinja earthquake studies were the (preliminary) aftershock locations that came from two different sources - the Croatian Seismological Survey (CSS) (e.g. Markušić et al., 2021; Tomac et al., 2021; Baize et al., 2022) and Herak and Herak (2023) (e.g. Sardeli et al., 2024). Žilić et al. (2025), using broadband data to create empirical Green's functions, derived a kinematic rupture model revealing a relatively small rupture length of less than 10 km, with a maximum slip of 5 m, and relatively short rupture duration of 5 s. This is consistent with the earlier results from Xiong et al. (2021), who used InSAR Sentinel-1 interferograms to derive a rupture model with a rupture length of 8.3 km and maximum slip of 3.5m.

2.2 Seismic network

Before the start of the Petrinja earthquake sequence, the Croatian seismic network had a relatively sparse configuration. Permanent stations operated by the Department of Geophysics at the University of Zagreb and the CSS covered the country, but the closest stations to the epicentre of the Petrinja earthquake were approximately 32 (RUJC) and 36 (MOSL) km away. Initially, the seismological monitoring of this earthquake sequence was hindered for several reasons – available instruments were already used to cover the Zagreb area following the March 2020 M_w 5.3 earthquake (Herak et al., 2022) and due to the COVID-19 pandemic and international travel restrictions, installation of new, temporary stations was delayed. Consequently, the network was densified on 4 January 2021 when the Department of Geophysics and colleagues from Italy's National Institute of Oceanography and Applied Geophysics (OGS) installed a temporary network (OP-Net) of five short-period instruments (Stipčević et al., 2021). Later, between mid-January and March 2021, an additional pool of 20 broadband instruments (and 20 accelerometers) were installed in the wider epicentral area by the CSS (PM-Net).

The deployment of OP-Net and PM-Net had a profound impact on data quantity and station coverage

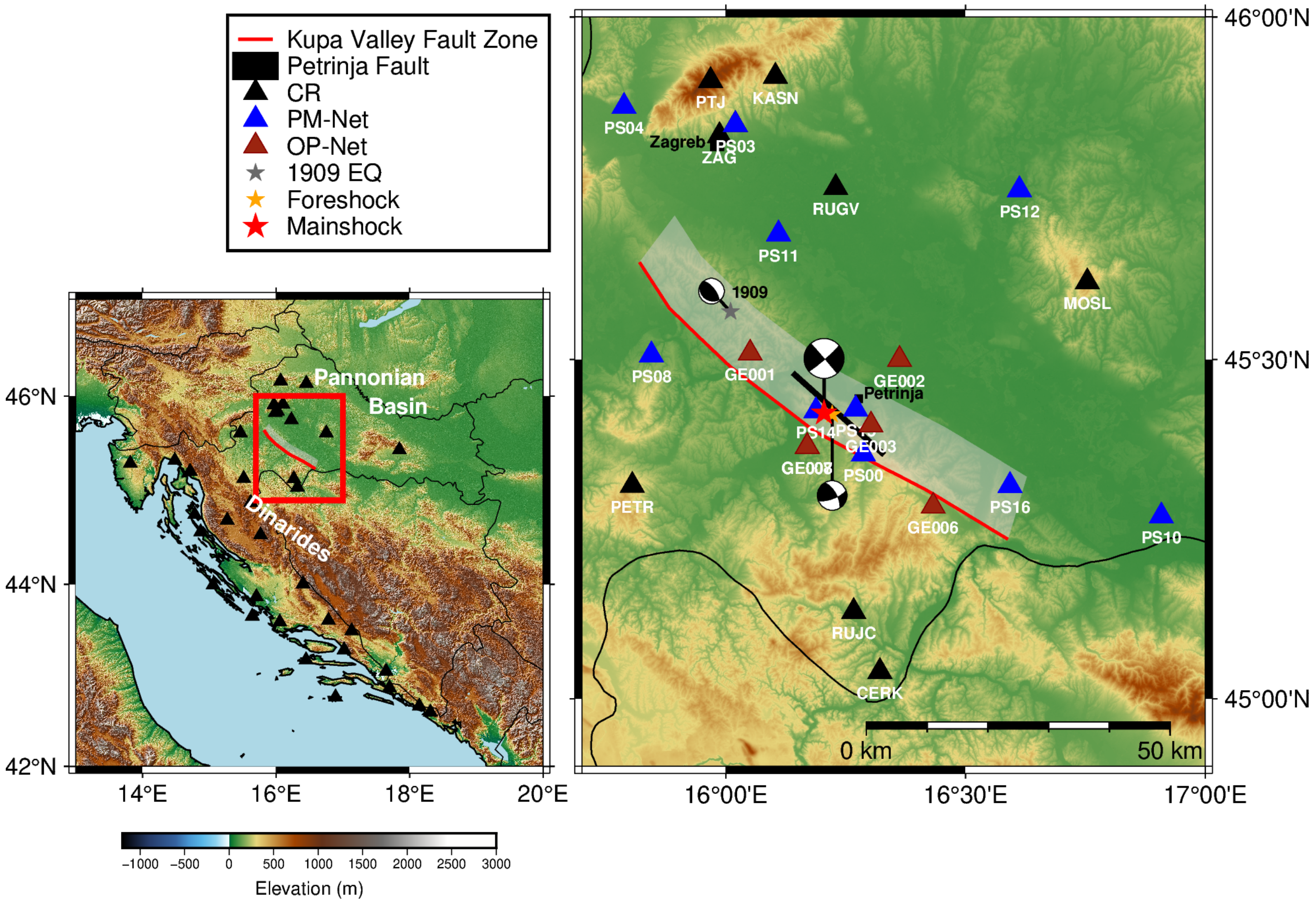

Figure 1 Seismic network in Croatia (left) before the onset of the Petrinja earthquake sequence and (right) after the temporary networks in Petrinja region were installed. OP-Net was installed on 4 and 5 January 2021. PM-Net was installed between mid January and March 2021. Locations of the foreshock (orange star), mainshock (red star), and historical 1909 earthquake (grey star) are plotted with their fault-plane solution FPS (Herak, 2025). Red line indicates Kupa Valley Fault Zone (Basili et al., 2020) while black line indicates causative Petrinja fault from Herak and Herak (2023).

quality. Herak and Herak (2023) report reducing location uncertainties by as much as 50% and show that before these deployments, the median confidence radius for epicentral coordinates was approximately 1 km, with focal depth uncertainties of up to 5 km. After the first additional stations were operational (OP-Net), the depth uncertainty dropped to around 2 km, and epicentral location errors were reduced to less than 0.7 km.

2.3 Seismic catalogues

This study benefits considerably from two very detailed, manually picked catalogues: the Croatian Earthquake Catalogue (CEC) (Herak et al., 1996), which represents the authoritative national seismic record for Croatia, compiled using routinely located epicentres by the CSS, and a catalogue covering the first six months of the sequence from the study by Herak and Herak (2023), referred to in the text as the Herak & Herak Catalogue (HHC). Notable differences exist between these two catalogues in the number of earthquakes located during the first six months of the sequence monitoring. This discrepancy can be attributed to the differences in methodology and analyst expertise: the CEC was compiled by multiple analysts with varying levels of experience, whereas the HHC was curated by a single experienced analyst who deliberately excluded events that were evidently challenging to locate with high certainty. These differences between manually curated catalogues highlight the advantages of ML-generated catalogues. Firstly, the amount of time it takes to create a manual catalogue for a months- to years-long active earthquake sequence is several months to a year while ML catalogue for the same earthquake sequence is produced in a matter of days, and secondly, ML techniques eliminate individual analyst biases and provide the ability to quantify the probability associated with each phase arrival, enhancing the overall reliability of the catalogue.

3 Data & Methods

3.1 Data

The continuous data used in this study come from the permanent Croatian Seismograph Network (CR) (University of Zagreb, 2001), which at the time consisted of 35 broadband, three-component stations, as well as two temporary networks: OP-Net and PM-Net, consisting of five short-period and sixteen broadband three-component stations, respectively. At its peak, the total number of stations reached 56, as the OP-Net instruments were removed on 21 April 2021. Data from the permanent network stations were mostly sampled with 50 Hz, while the temporary network stations sampled with 250 Hz (OP-Net) and 100 Hz (PM-Net). The analysed period spans from 28 December 2020, to 30 November 2022. For each available station, the raw waveforms are only pre-processed by removing the mean and filling the data gaps with zeros.

3.2 Phase picking and associator

For earthquake and seismic phase detections we employ a widely used EQTransformer picker (Mousavi et al., 2020) trained on the INSTANCE dataset (Michelini et al., 2021) through Seisbench (Woollam et al., 2022), a toolbox which allows us to easily use different pickers with their 'non-native' training datasets. The probability thresholds for earthquake detection, P waves, and S waves were set to 0.05, meaning if our picker has a confidence value above 0.05 assigned to a pick, it treats it as a phase arrival. Further, EQTransformer processes 60-s-long data segments using moving windows with adjustable overlaps, and Pita-Sllim et al. (2023) showed that detection of P and S arrivals strongly depend on the phases' start time within this 60 s window. We therefore set the overlap length of 50 s, which, in combination with P- and S-probability thresholds, should balance detection rate and false positives (Pita-Sllim et al., 2023). The low P- and S-probability thresholds do lead to the increase in false positive detections; however, these picks will later be filtered out by association and relocation process. For phase association we use the PyOcto phase associator (Münchmeyer, 2024) based on space-time partitioning. The preliminary event locations are calculated using a homogeneous halfspace with $v_p = 6.0$ km/s and $v_s = 3.42$ km/s. The homogeneous halfspace assumption should work as a first step as it is sufficient for regions with shallow seismicity (Münchmeyer, 2024). Since the number of stations in the network changed during the analysed period, we used two sets of parameters for the association process. For the first 8 days of the sequence (28 December 2020 – 4 January 2021), i.e. before first stations of the temporary network OP-Net were installed, we required a minimum of five picks per event with at least two stations with P and S picks. After 4 January 2021, we increased this requirement to a minimum of seven picks out of which there is a minimum of three P and three S picks per event and at least three stations should have both P and S waves detected.

3.3 Earthquake location and relocation

The preliminary PyOcto earthquake locations are further refined using NonLinLoc (NLL) (Lomax et al., 2000), applying source-specific station travel-time corrections (SSST, Lomax and Savvaidis, 2021) to improve location accuracy. In addition, the probability output of the EQTransformer for each pick was used so that picks with higher probability were assigned smaller pick time uncertainties during event location. For initial NonLinLoc, we used the one-dimensional (1D) velocity model based on Herak and Herak (2023), which is tailored to the seismic characteristics of the study region. For the NLL-SSST relocations, we iteratively generate SSST corrections, which vary smoothly within a 3D volume to provide a source-position dependent correction for each station and phase type. We use smoothing distances of 64, 32, 16, and 8 km and only use events in our final catalogue which have arrival data at one of the nearby temporary networks (PM and OP-Net), pick probability higher than 0.6, and have a number of read phases ≥ 15. We further utilised HypoDD (Waldhauser and Ellsworth, 2000) to improve relative accuracy of event locations, however no substantial improvements in relative locations were achieved. This indicates that the initial locations, obtained using source-specific station terms, already provide a self-consistent representation of the relative event geometry. Finally, in our catalogue, we only include events from our study region (15.7°–17.0°E, 44.9°–46.0°N) (Figure 1).

4 Results

4.1 Petrinja Earthquake Sequence Machine Learning Catalogue (PESMLC)

EQTransformer analysis detected a total of 8,948,261 seismic phases, consisting of 6,588,039 P phases and 2,365,691 S phases. After applying association criteria to the detected phases, we retained 711,251 valid picks (51% P phases, 49% S phases), demonstrating a balanced detection capability for both seismic phases. From these associated picks, the Petrinja Earthquake Sequence Machine Learning Catalogue (PESMLC) was made consisting of 41,989 events. Figure 2 illustrates the number of events in our catalogue compared to the total number of initial picks detected by EQTransformer and the number of associated picks that were ultimately used to build the catalogue. It can be observed that, after the initial weeks of the sequence, there is a significant decrease in both the number of detected and associated picks, reflecting the stabilization of the seismic activity over time. A notable peak in initial picks during April 2022 corresponds to correctly identified seismic arrivals most likely from the Berkovići earthquake sequence in Bosnia and Herzegovina (Dasović et al., 2024), which occurred at that time. However, as this sequence is outside the scope of our studied region, these picks were not associated. The temporal distribution of events in the PESMLC follows the expected aftershock decay pattern (Figure 2). This suggests that our machine learning model successfully captures the temporal evolution of the aftershock sequence, providing a valid and comprehensive dataset.

Figure 3 shows detailed spatial and magnitude distribution of events in the PESMLC. Several distinct seismicity clusters emerge from our catalogue. The majority of the seismicity is clustered around the primary Petrinja fault zone. We identify additional four smaller clusters (Figure 3a), three of them (I–III) associated with Petrinja earthquake sequence and the aftershock sequence of the 22 March 2020 Zagreb M_w 5.3 earthquake (Herak et al., 2022) (IV). The main cluster exhibits a

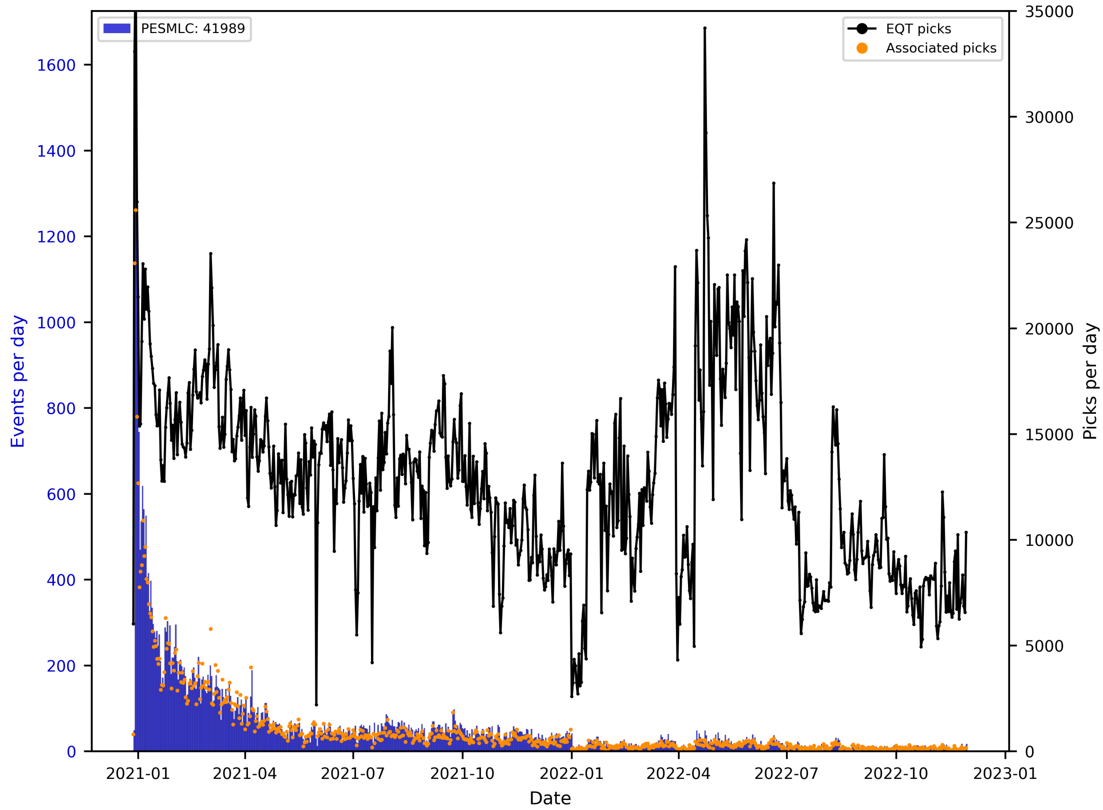

Figure 2 Number of events in the Petrinja Earthquake Sequence Machine Learning Catalogue (PESMLC) (blue, left vertical axis) with superimposed number of initial (black, right vertical axis) and associated (orange) picks.

clear separation along NE–SW axis, distinctly visible in cross-section views (Figure 3c,d), with the NW segment showing slightly deeper seismicity.

To quantify the spatial concentration of seismicity, we computed the mean latitude, longitude, and depth for all events in the catalogue, along with their standard deviations. Our analysis reveals that 64% of the seismicity is situated within one standard deviation of these mean earthquake locations, i.e. between 16.08°–16.38°E, 45.27°–45.53°N, and between 4.5 and 14 km depth as shown by the kernel density estimates (KDE) adjacent to the cross-section plots, suggesting a shallow-crustal earthquake sequence. KDE of the longitude distribution also indicates two distinct clusters. Figure 3b shows the local earthquake magnitude distribution of the events in the catalogue in time. Local earthquake magnitudes were calculated using the formula

$$M_{\mathrm{CR,L}} = \log A + 2.094 \log(\Delta^\circ) + 2.190, \qquad (1)$$

where A is the maximum S-wave amplitude of ground velocity measured in $\mu\mathrm{m/s}$, and Δ° is hypocentral distance in degrees (Herak, 2020). This empirical relationship has been calibrated for the wider area of Croatia and is standardly used to estimate local magnitude in the Croatian Seismic Catalogue. Local magnitudes were calculated for each station, and the final event magnitude was estimated as the mean value across all stations. Mean and median magnitudes are 0.66 and 0.71, respectively, suggesting that the majority of events in the catalogue have magnitudes below 1, which is to be expected, especially when using machine learning algorithms. It is noteworthy that events with magnitudes as low as −2 are detected only during the deployment period of the OP-Net temporary network (Figure 3b), highlighting the enhanced sensitivity achieved by installing instruments in close proximity to the fault zone. Note that magnitudes were calculated automatically across all 41,989 events without individual quality verification of each amplitude pick. This automatic approach likely results in an underestimation of local magnitudes, primarily due to potential inaccuracies in automatically picking maximum amplitudes, particularly in low signal-to-noise conditions.

4.2 Validation

To validate our catalogue, we compare it with manual catalogues from Herak and Herak (2023) and from the CSS. In our comparison, we define a matched event as one for which the time difference between PESMLC and the manually detected event's origin time is less than 2 seconds. Missed events are events present in manual catalogues but absent in PESMLC. Finally, events present in PESMLC but absent in the manual catalogue are regarded as new identifications.

4.2.1 Validation - Comparison with Herak & Herak (2023) Catalogue

We first compare our catalogue with the Herak and Herak (2023) catalogue (referred to as HHC). The comparison spans the first 6 months of the sequence (28 December 2020 – 28 June 2021), and, for consistency, our catalogue was spatially filtered to match the geographic extent of the HHC, selecting only events within

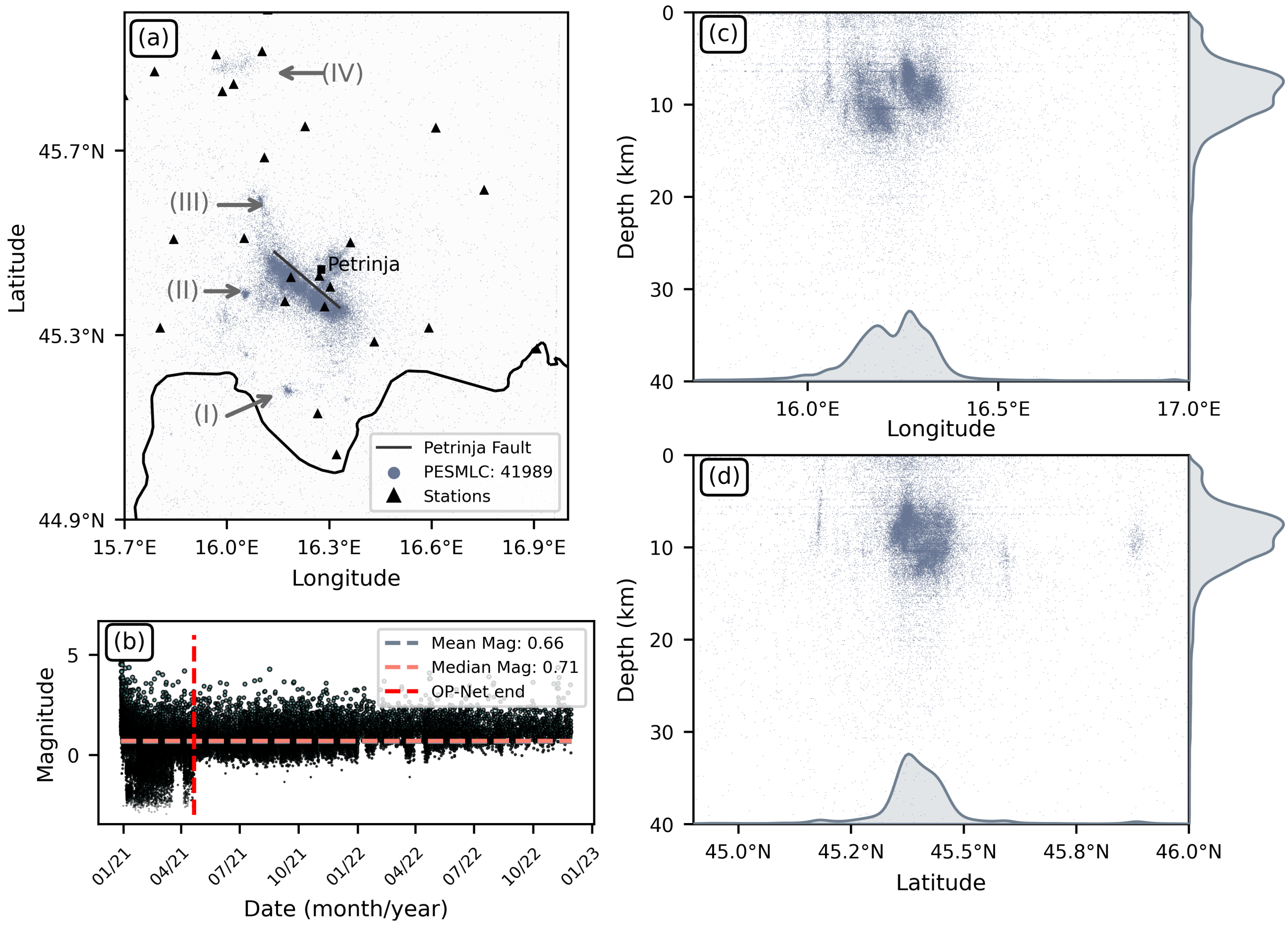

Figure 3 (a) Map view, (b) magnitude distribution, and (c and d) vertical cross sections of events in PESMLC. The vertical cross sections show kernel density estimation (blue curves, right and bottom) for depth vs longitude (c), and depth vs latitude (d) distribution.

the region bounded by 15.7°–16.7° E, 44.9°–45.75° N. In this time window and region, there are 28,060 events in PESMLC and 13,770 events in HHC.

Our comparative analysis results in 13,188 matched events (96% of HHC events), 582 missed, and 14,872 newly identified events. Among the 582 events that were missed, 110 events in HHC were originally located using fewer phases than required by our association criteria (5 phases before 04/01/2021, 7 phases after 04/01/2021). If we exclude these 110 events from our comparison, we arrive at a remarkable 97% confirmed match of the HHC catalogue. Map view of seismic events for both catalogues (Figure 4a) shows that PESMLC correctly locates and clusters seismic activity, both around the main fault and for the smaller clusters (I–III in Figure 3). We see that the majority of missed events (Figure 4b) happened in the first few days of the sequence—primarily due to the sheer amount of the events and the sparser network during the initial phase of the sequence. The latitude distribution of seismicity in PESMLC and HHC is consistent. Similarly, the longitude distribution matches well; however, the clear bimodal pattern observed in HHC appears slightly smoothed in PESMLC. Additionally, the depth distribution in PESMLC is both shallower and narrower than that in HHC.

Further, we analysed the statistical differences in matched events for latitude, longitude, depth, and magnitude. The mean differences in latitude and longitude are relatively small, at 0.8 km (0.007°) and 0.6 km (0.008°), respectively, indicating good horizontal agreement between catalogues. The observed mean depth difference of 2.16 km, suggests slightly shallower event locations than reported in HHC. This difference is primarily a result of variations in the number and relative proportion of S-wave arrivals between the two catalogues. The PESMLC contains a comparable number of P- and S-wave picks (259,494 P and 257,923 S), whereas the manual catalogue is dominated by P-wave arrivals (174,526 P and 79,419 S). This more balanced phase distribution in the PESMLC better constrains hypocentral depth, resulting in a higher-quality catalogue. A similar effect has been reported by Fonzetti et al. (2025). The mean magnitude difference of 0.1 suggests that magnitudes in HHC are, on average, slightly higher than those in PESMLC, likely due to the automated amplitude picking in PESMLC compared to manual amplitude selection in HHC. Additionally, Table 1 shows the improvements of our results after the installation of the additional stations on 4 January 2021, with the event location aligning with the uncertainty range reported in Herak and Herak (2023).

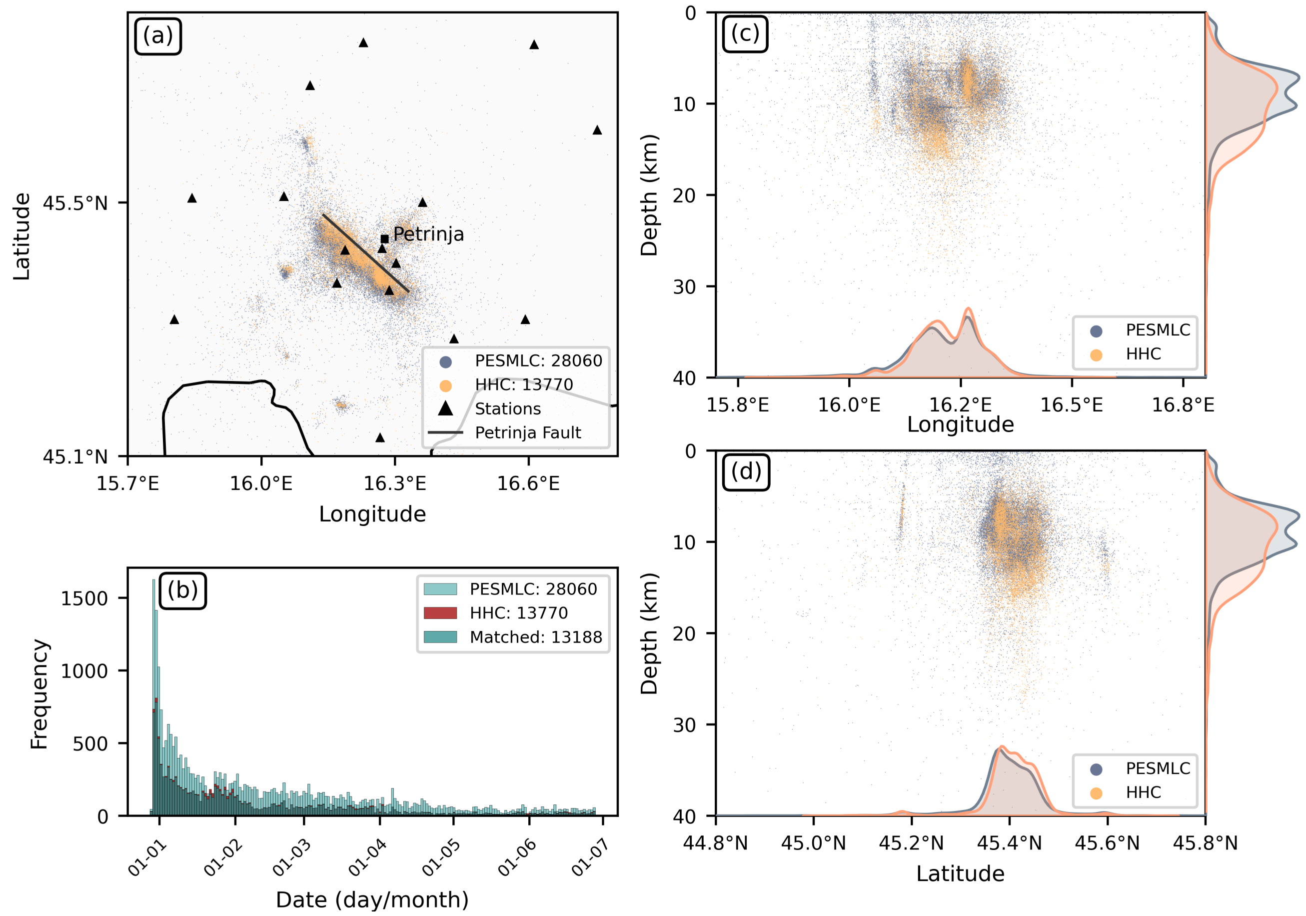

Figure 4 Comparison with the Herak and Herak (2023) catalogue (HHC) for the first six months of the sequence. (a) Map view of the seismic events from the Petrinja Earthquake Sequence Machine Learning Catalogue (PESMLC; blue) and HHC (orange). (b) Temporal distribution of the number of events in PESMLC (blue) and HHC (red) with overlaid matched events (green). Each bin represents the number of events per day. (c), (d) vertical cross sections comparing the depth distribution of the events in both catalogues against (c) longitude and (d) latitude. Kernel density estimates adjacent to the panels show the difference in the event density between PESMLC (blue) and HHC (orange).

	HHC		CEC	
	Before 04/01/21	After 04/01/21	Before 04/01/21	After 04/01/21
Δlat (km)	1.11	0.81	1.70	0.63
Δlon (km)	0.68	0.56	0.45	0.39
Δdepth (km)	4.07	1.62	1.66	0.73
Δmag	-0.05	0.16	0.03	0.15

Table 1 Effect of network densification on mean latitude, longitude, depth, and magnitude differences for matched events between manual catalogues (HHC and CEC) and the Petrinja Earthquake Sequence Machine Learning Catalogue (PESMLC).

4.2.2 Validation - Comparison with Croatian Earthquake Catalogue (CEC)

Next we compare PESMLC with the most recent Croatian Earthquake Catalogue (referred to as CEC) from the CSS, covering the full duration of our study period and study region (15.7° – 17.0° E, 44.9°–46.0° N). In this time window, CEC consists of 22,958 events. Our analysis results in 19,489 matched events (85%), 3474 missed, and 22,500 new events. Out of the 3474 missed events, 629 were originally located using fewer phases than our association requirements. Excluding these events increases the match rate to 87% between the two catalogues. We again see a strong agreement between the two catalogues in spatial and temporal distribution (Figure 5), consistent with our previous comparison to HHC. Notably, the distinct bimodal longitudinal distribution of seismicity clearly visible in the CEC catalogue is again smoothed in the PESMLC. The apparent smoothing of the bimodal longitudinal distribution observed in PESMLC compared to CEC and HHC results from PESMLC's additional detections, which effectively populate the spatial gaps between previously distinct clusters. The depth distribution of events in PESMLC again appears slightly shallower and narrower compared to CEC. We further assessed the agreement between 19,489 matched events in the PESMLC and CEC by analysing statistical differences in latitude, longitude, depth, and magnitude. Horizontal differences in event locations are generally small, with mean latitude and longitude differences of 0.85 km (0.007°) and 0.4 km (0.005°), respectively. The mean depth difference is 0.93 km, indicating slightly shallower event locations com-

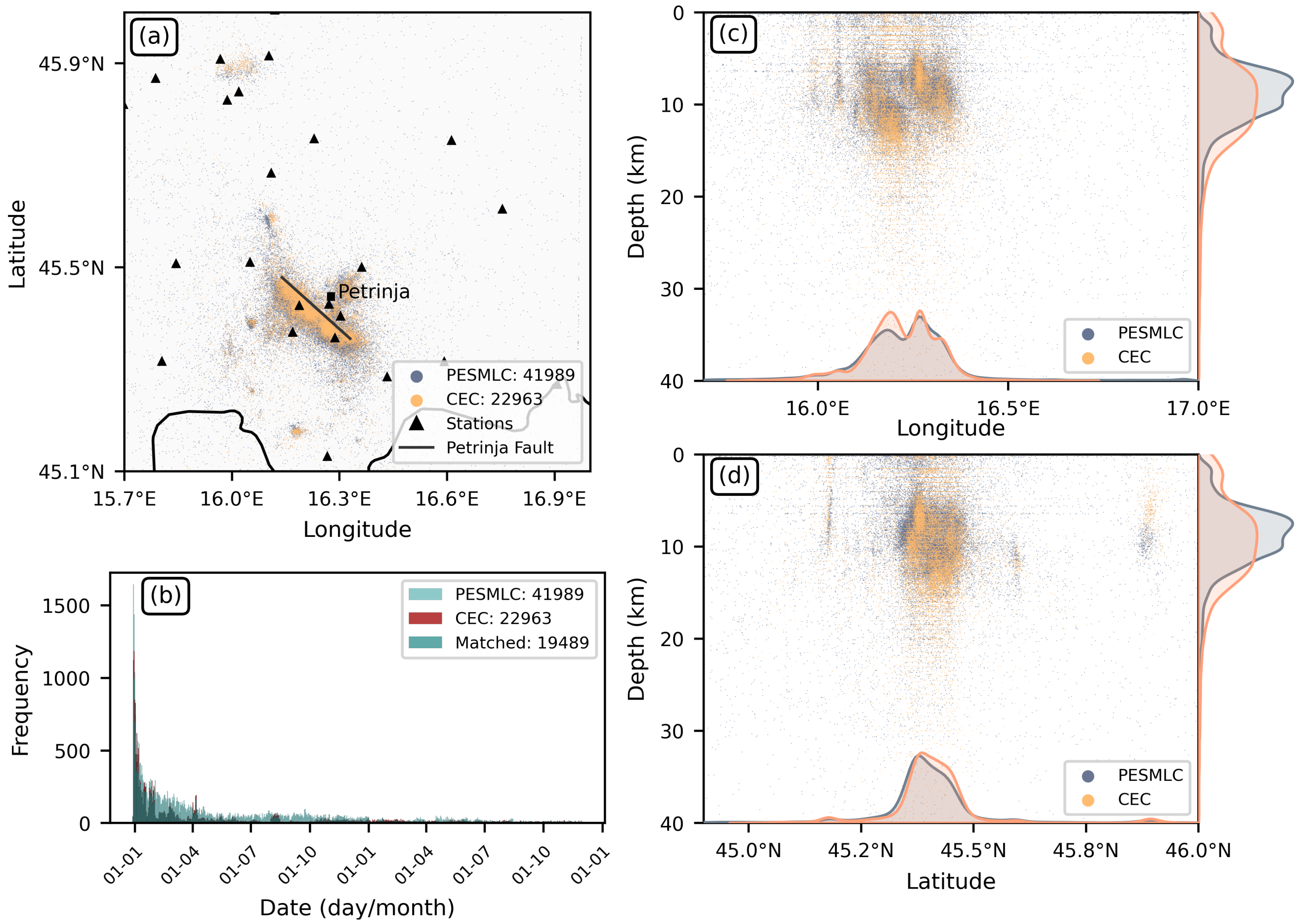

Figure 5 Comparison between PESMLC and the Croatian Earthquake Catalogue (CEC). (a) Spatial distribution map. (b) Temporal distribution comparison. (c,d) Vertical cross-sections highlighting differences in depth distributions. Kernel density estimations (KDE) adjacent to each panel illustrate event-density differences between PESMLC (grey) and CEC (orange), highlighting spatial variations in event detections.

pared to the manual catalogue, with overall improvements in location and magnitude agreement following the installation of the temporary network (Table 1).

5 Discussion

The comprehensive comparison of PESMLC with manually curated catalogues (HHC and CEC) has highlighted the capabilities and limitations of ML-based seismic event detection. The analysis confirms that automated approaches capture a significantly larger number of events (e.g. Becker et al., 2024; Sugan et al., 2023; Cianetti et al., 2021; Fonzetti et al., 2025), including previously undetected microseismicity, while maintaining strong agreement with manually analysed data, especially for moderate magnitude events. However, inherent limitations related to overlapping events, minimum associator criteria, and phase-picking accuracy warrant consideration for future methodological improvements.

5.1 Matched events

Encouragingly, for both catalogues, there is a high number of matched events, with 96% and 85% for HHC and CEC, respectively, indicating that our approach successfully detects a high percentage of significant events. Notably, when we compare HHC and CEC in the same way, i.e. characterising an event as matched if it is within 2 seconds of an event in HHC, focusing only on the study area from Herak and Herak (2023), CEC only matches 75% of the events. Low average differences in latitude and longitude between the PESMLC and manual catalogues support the decision to prioritise temporal, rather than strict spatial, matching in the comparison. Although a small number of matched events exhibit larger spatial offsets, these are retained in the catalogue. Such outliers likely reflect increased location uncertainty, primarily due to the limited station geometry, particularly during the first few days of the sequence when only stations of the initial network configuration were available. Nevertheless, the ML-based picking and association successfully identify these events and constrain their origin times, justifying their inclusion despite less well-resolved hypocentral locations. In total, out of the 41,989 events in PESMLC, there are 22,553 events that are matched with events in either HHC or CEC. In addition to horizontal agreement, systematic differences on the order of 2 km are also observed in hypocentral depth. For events matched with the catalogue of Herak and Herak (2023), depths obtained in this study are generally shallower, predominantly ranging between 4.5 and 14 km, compared to depths extending to 18 km reported in the manual analysis. This discrep-

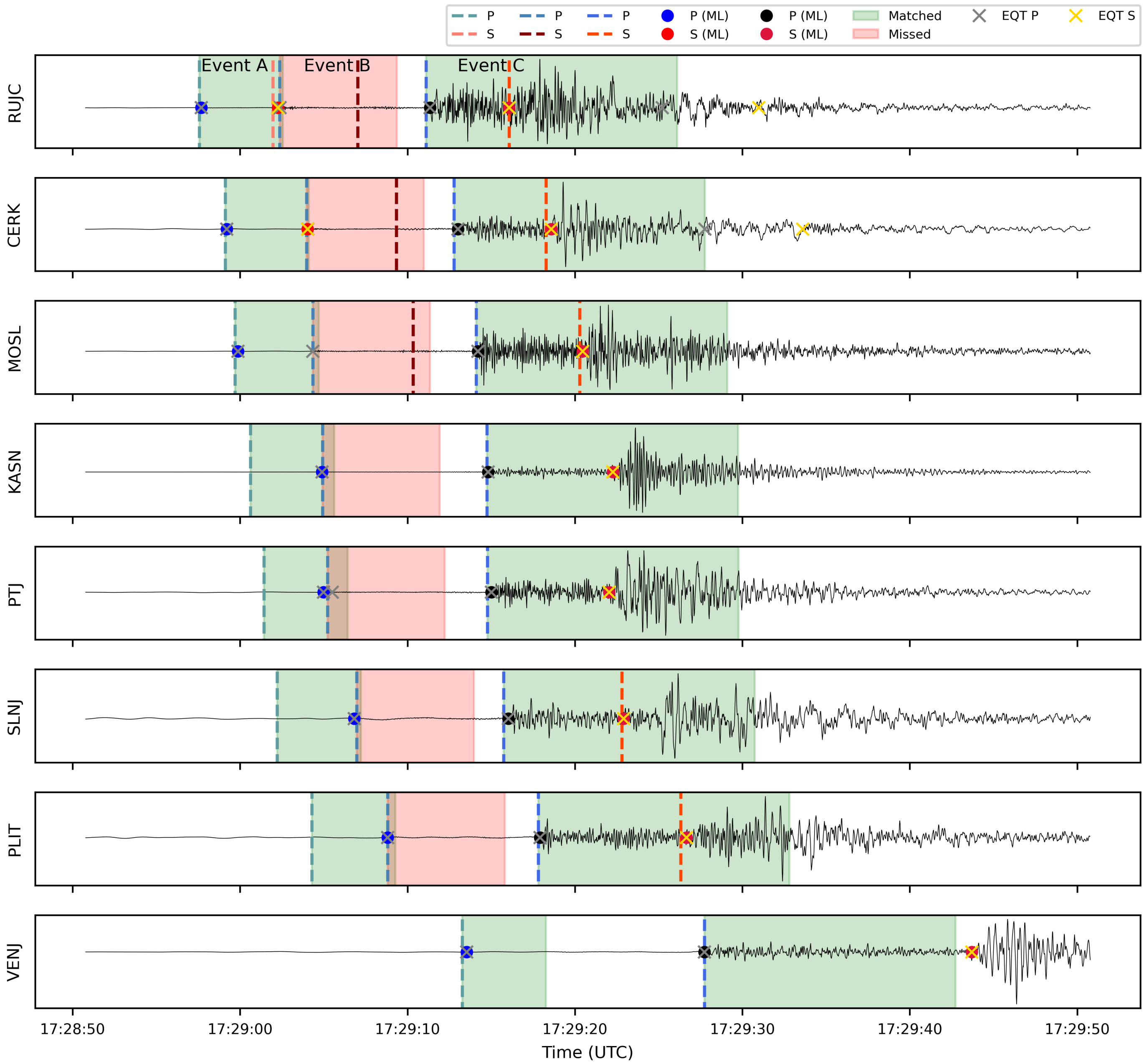

Figure 6 Example of missed event detection: $\mathrm{M_{CR,L}} 3.08$ event (shaded red) representing the largest missed event. Shown are one minute seismogram across nine stations showing three closely spaced events (Event A,B,C). Vertical lines indicate manual phase arrivals from HHC. Coloured dots represent associated P (blue) and S (red) picks used for PESMLC and crosses represent identified P (grey) and S (yellow) phases by EQTransformer. Matched events (Event A and C) between HHC and PESMLC are marked as green and the missed event, Event B, is shaded red.

ancy likely reflects differences in phase picking, station coverage, and location methodology, particularly the improved balance of P- and S-phase picks in the ML catalogue, which enhances depth resolution. The resulting shallower depth distribution reduces the need to invoke unusually deep seismicity or elevated-temperature brittle behaviour, as previously suggested (Herak and Herak, 2023), and instead indicates that seismicity during the sequence may be largely confined to the upper crust.

5.2 Missed events

Further, looking at the magnitude distribution of missed events, we see that out of 582 missed events from HHC, there are two missed events with magnitude greater than $\mathrm{M_{CR,L}} 3$, 6 events with magnitudes $2 \leq \mathrm{M_{CR,L}} < 3$, 63 events with $1 \leq \mathrm{M_{CR,L}} < 2$, 136 events with $0 < \mathrm{M_{CR,L}} < 1$, and 375 events for which HHC gives magnitude 0 (i.e. could not be estimated). The largest missed event is a $\mathrm{M_{CR,L}} 3.08$ earthquake on 29 December 2020 at 17:28:54 (UTC), before additional stations were installed. There are two possibilities for these missed events. This could occur due to the EQ-Transformer failing to detect them or to their exclusion during our phase association process because they don't meet our minimum requirements. Figure 6 shows the 1 min seismogram from nine stations. During this 1 min, there are three events in HHC – Event A ($\mathrm{M_{CR,L}} 2.97$) with origin time at 17:28:50, Event B ($\mathrm{M_{CR,L}} 3.08$) occur-

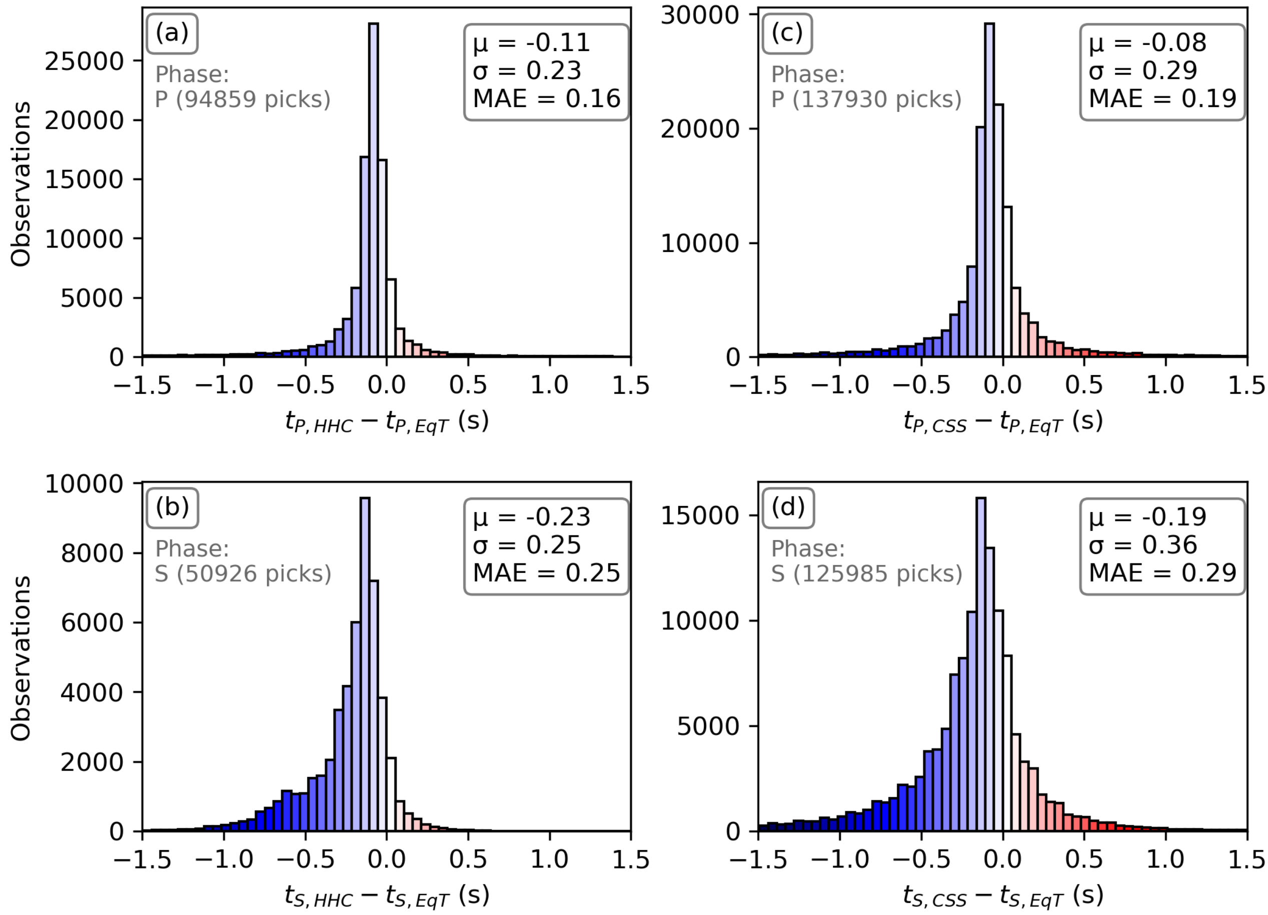

Figure 7 Distribution of time differences between manual and ML picks. (a), (b) Comparison between picks for (a) P phase and (b) S phase used for HHC and associated ML picks. (c), (d) Comparison between manual picks in CEC with associated ML picks. Blue bars indicate cases where manual picks precede ML picks, while red bars show cases where ML picks precede manual picks.

ring at 17:28:54, and Event C ($M_{CR,L}3.66$) at 17:29:04. Events A, B, and C are closely located, with mutual distances ranging from approximately 1.4 to 3.1 km, depths of 7.72, 24.32, and 1.79 km, respectively, indicating that they originated from the same area. We can see that Event C, dominating the seismograms, is correctly matched. However, phases from two distinct, closely spaced events (Events A and B) are combined by PESMLC into a single associated event and matched with Event A from HHC. For stations RUJC and CERK, P phases for all three events are correctly identified, while S phases are only identified and associated for Events A and C. For station MOSL, P phases are again correctly identified for all three events; however, the S phase is only correct for Event C. For stations KASN, PTJ, SLNJ, and PLIT, P phases of Events B and C are identified; however, P phases of Event B are incorrectly associated with the event that was matched with Event A. Nevertheless, Event B could not be associated and included in PESMLC because it does not satisfy our minimum associator requirements, as no S phases are identified for this event. Event A, even if we remove the incorrectly associated picks, still satisfies the minimum association requirements. This example highlights a common challenge for automated algorithms during a dense seismic sequence, particularly within short inter-event intervals with overlapping codas which was common in the first few days of this sequence. It underscores the critical importance of training ML pickers on datasets that include overlapping events (Kim et al., 2022), crucial to study seismic swarms. However, most missed events from manual catalogues occur due to not meeting the minimum phase association requirements, suggesting that improving network density is an effective solution, as it allows more events to meet the minimum phase association requirements regardless of whether picks are generated automatically or manually. This is supported by our finding that, out of 71 missed events with magnitudes greater than $M_{CR,L}1$ in HHC, only 21 occurred after the OP-Net temporary network became fully operational on 5 January 2021. In the case of a continuously sparse seismic network, lowering minimum phase association requirements can be a solution; however, it comes with an increase in the number of new identifications, often with poor quality solutions.

Similarly, for the complete time period of the study, when comparing with CEC, there are 3,469 (15%) missed events. Out of these, less than 1% (23 events) have magnitudes greater than $M_{CR,L}2$, 26% (914) have magnitudes between $M_{CR,L}1$ and $M_{CR,L}2$ and approximately 73% (2,532) of missed events have magnitudes below $M_{CR,L}1$.

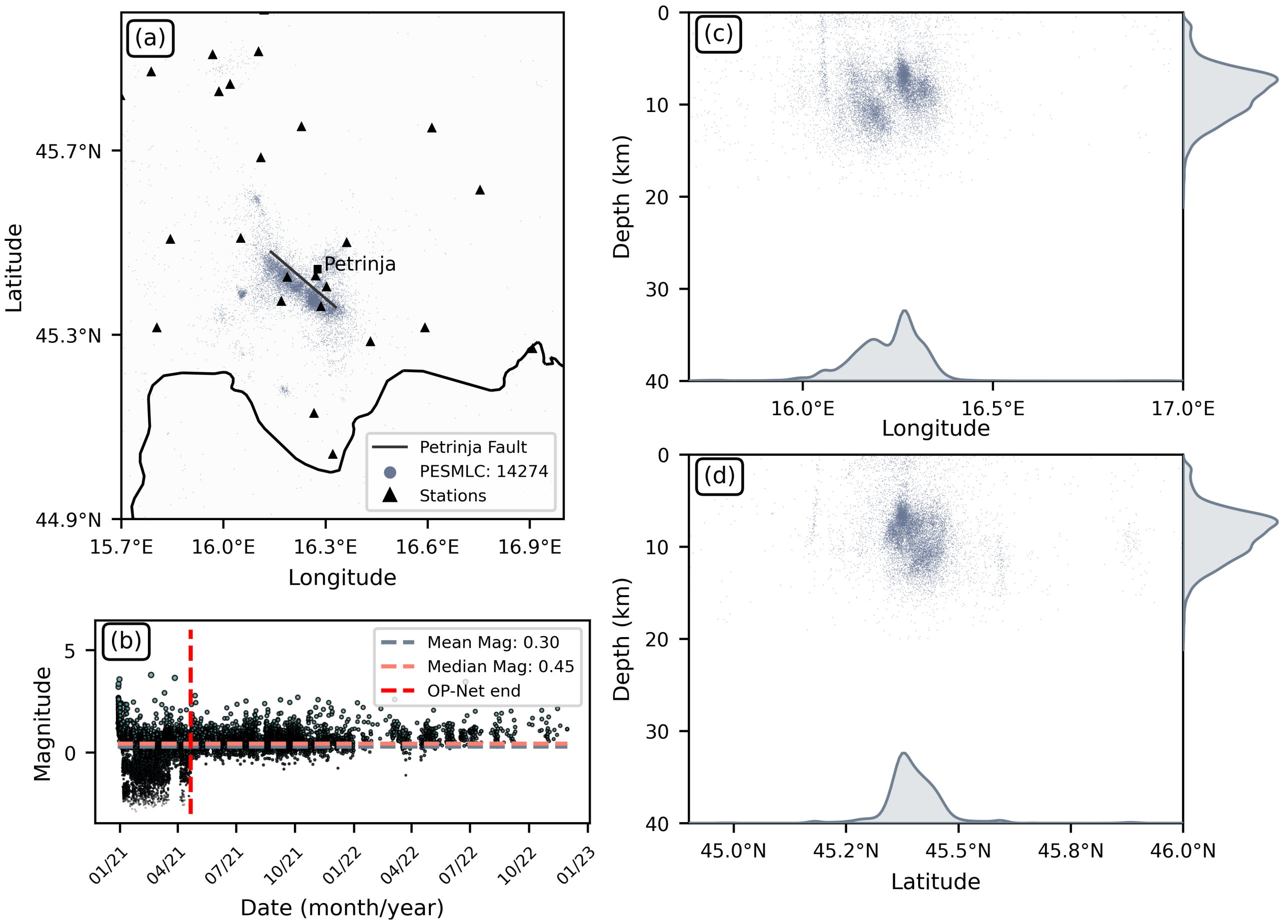

Figure 8 Spatial and magnitude distribution of 14,274 new events in PESMLC that satisfy our quality criteria and are undetected in the manual catalogues.

Figure 6 also highlights the difference in phase arrival picking times between manual and ML methods. These differences, combined with differences in the velocity model and location method, affect the estimated earthquake locations. The comparative analysis between manual and ML picks (Figure 7) shows these systematic differences in picking times. We compare manual picks and associated ML picks at each station, and our analysis shows that ML picks, both P and S phase, appear slightly delayed compared to HHC and CEC manual picks. When comparing with manual picks from HHC, P phases are picked on average 0.11 s earlier by human analyst, and S phases, on average, 0.23 s earlier. Picks are slightly closer when we compare them with manual picks used for CEC, with ML P phases on average 0.08 s delayed, and S phases 0.19 s delayed. It is worth noting that HHC was picked by one experienced analyst and CEC was picked by several analysts from the CSS with varying level of experience. This could explain the more consistent time discrepancy, especially in picking the S phase. These time delays are not uncommon for ML algorithms. Sugan et al. (2023) report P phase differences within ± 0.1 s, and S phase delays by around 0.1 to 0.3 s compared to manual picks.

5.3 New events

A primary concern when using ML algorithms is the reliability of (newly) identified events, particularly the distinction between genuine earthquakes and false detections. Here, this issue is mitigated by the availability of two detailed manual catalogues, which serve as a reference for validation. However, the new identifications more than double the number of detected events, both in comparison with HHC for the first six months of the sequence and compared with CEC for the entire period of our study. This increase in detected events is consistent with previous studies employing ML techniques, which typically report at least two to three times more detected events compared to manual catalogues (e.g., Becker et al., 2024; Sugan et al., 2023; Cianetti et al., 2021). To isolate likely genuine events and reduce noise, the newly identified events are filtered based on quality criteria from the location process: an azimuthal gap smaller than 180°, a depth shallower than 20 km, and a major axis length of the 3D confidence ellipsoid of the hypocentral location of less than 10 km. Following this filtering, out of the 19,436 events in the PESMLC that are considered newly identified, 14,274 events satisfy these criteria (Figure 8).

The spatial distribution of newly identified events provides compelling evidence that these are genuine seismic events rather than false detections. New identifications overwhelmingly concentrate along the same fault structures and clusters defined by the manually verified matched events, with smaller-magnitude new events (Figure 8b) filling in spatially between larger, manually detected ones rather than appearing at random locations. Random false detections — whether from noise, instrument artefacts, or associator errors — would not be expected to reproduce this fault-controlled spatial pattern. The consistency between the spatial distribution of new and matched events therefore strongly supports the physical reality of the newly detected (micro)seismicity and suggests that PESMLC is recovering genuine small-magnitude seismicity that was below the detection threshold of manual analysis, rather than introducing noise into the catalogue.

5.4 Magnitude of completeness

The magnitude of completeness ($\mathrm{M_c}$) of a seismic catalogue defines the minimum magnitude above which the seismic catalogue is considered complete, meaning that all earthquakes of equal or greater magnitude are consistently detected by the seismic network. $\mathrm{M_c}$ is typically determined by analysing the frequency-magnitude distribution (FMD) of recorded events and identifying the point where the catalogue becomes complete, usually where the distribution begins to follow the expected Gutenberg-Richter law. As ML-generated seismic catalogues, in general, are expected to detect more seismicity than their manual counterparts, especially lower magnitude seismicity, we would expect $\mathrm{M_c}$ values for such catalogues to be significantly lower than for manual ones. However, manually curated catalogues may also achieve lower $\mathrm{M_c}$ values, as analysts can identify and associate very small events recorded on only a limited number of stations. This is reflected in our comparison, where 110 missed HHC events and 629 missed CEC events were associated using fewer phases than required by our association criteria. To evaluate this, $\mathrm{M_c}$ is estimated using three methods implemented in the SeismoStats package (Mirwald et al., 2026) – the b-value stability (MBS) method (Cao and Gao, 2002), the Maximum Curvature method (MAXC) (Wiemer and Wyss, 2000; Woessner and Wiemer, 2005), and the Kolmogorov-Smirnov (K-S) method (Clauset et al., 2009; Mizrahi et al., 2021) – for the complete PESMLC, a quality-filtered subset of PESMLC (retaining only matched events and newly identified events satisfying our quality criteria; see Section 5.3), HHC, and CEC (Figure 9).

For the first six months of the sequence, results are consistent with expectations: b-values are consistent across catalogues ($b = 0.87$ for complete PESMLC, $b = 0.86$ for filtered PESMLC, and $b = 0.88$ for HHC), and $\mathrm{M_c}$ values obtained using all three methods are lower for both PESMLC variants than for HHC. Specifically, for the complete PESMLC, $\mathrm{M_c}$ ranges from 0.90 (MAXC) to 1.05 (MBS) and 1.10 (K-S), and for the filtered PESMLC from 0.80 (MAXC) to 1.05 (MBS) and 1.10 (K-S), whereas for HHC all three methods converge on $\mathrm{M_c} \approx 1.1$. The slightly lower MAXC estimate for the filtered catalogue (0.80 vs 0.90) reflects the removal of low-quality detections that artificially inflate the peak of the FMD, shifting the maximum toward lower magnitudes.

When considering the full study period, a more complex pattern emerges. For CEC, $\mathrm{M_{c,MAXC}} = 1.10$, $\mathrm{M_{c,MBS}} = 1.06$, and $\mathrm{M_{c,KS}} = 1.30$ ($b = 0.95$). For the complete PESMLC, the estimated $\mathrm{M_c}$ is highly method-dependent. While MAXC remains low at $\mathrm{M_{c,MAXC}} = 0.90$, the MBS and K-S methods produce substantially higher values ($\mathrm{M_{c,MBS}} = 1.79$, $\mathrm{M_{c,KS}} = 1.20$, $b = 0.86$), exceeding even the manual catalogue results. However, when the analysis is repeated on the quality-filtered PESMLC, this discrepancy largely disappears ($\mathrm{M_{c,MAXC}} = 0.90$, $\mathrm{M_{c,MBS}} = 1.02$, $\mathrm{M_{c,KS}} = 1.10$, $b = 0.91$), with all three methods now converging to values comparable to, or lower than, those of the manual catalogues. This demonstrates that the elevated $\mathrm{M_c}$ estimates for the complete PESMLC are primarily driven by low-quality detections rather than genuine network incompleteness. Once these are removed, the filtered catalogue is statistically more complete than the raw one, despite containing fewer events.

The fact that the three methods still do not fully converge in the filtered catalogue ($\mathrm{M_{c,MAXC}} = 0.90$ vs $\mathrm{M_{c,KS}} = 1.10$) is consistent with the known statistical behaviour of these estimators. Both the MBS and K-S methods impose criteria that become progressively stricter with increasing catalogue size (Mirwald et al., 2026), as the theoretical uncertainty of the b-value decreases with the square root of the number of events, and the K-S test becomes sensitive to minor deviations from the idealised exponential distribution that are negligible in practical terms. This sensitivity is an inherent property of the methods rather than a reflection of true catalogue incompleteness, and its effect is amplified in large ML-generated catalogues. Consequently, we adopt $\mathrm{M_c} = 1.10$ as a conservative working threshold for the filtered PESMLC, consistent across the K-S and MBS estimates for both time periods, and use this value for subsequent analyses.

These results highlight two important practical lessons for $\mathrm{M_c}$ estimation in ML-generated catalogues. First, raw event counts should not be used as input to completeness analysis without prior quality filtering, as low-quality detections can influence strict estimators, such as MBS and K-S, to produce artificially high $\mathrm{M_c}$ values. Second, when multiple methods disagree substantially, quality filtering provides a diagnostic: if filtering resolves the disagreement, the cause was detection quality rather than network incompleteness; if disagreement persists, the catalogue may genuinely be incomplete at lower magnitudes.

This highlights the importance of carefully selecting the $\mathrm{M_c}$ estimation method when analysing large, ML-generated catalogues, as different approaches may yield substantially different completeness thresholds. Further investigations of similarly long and well monitored earthquake sequences, particularly those analysed using ML methods, are therefore needed to refine and improve current $\mathrm{M_c}$ estimation methods.

5.5 Aftershock decay

The temporal decay of aftershock activity is analysed using the Omori–Utsu law (Utsu et al., 1995), also referred to as the modified Omori law:

$$n(t) = \frac{K}{(t+c)^p}, \tag{2}$$

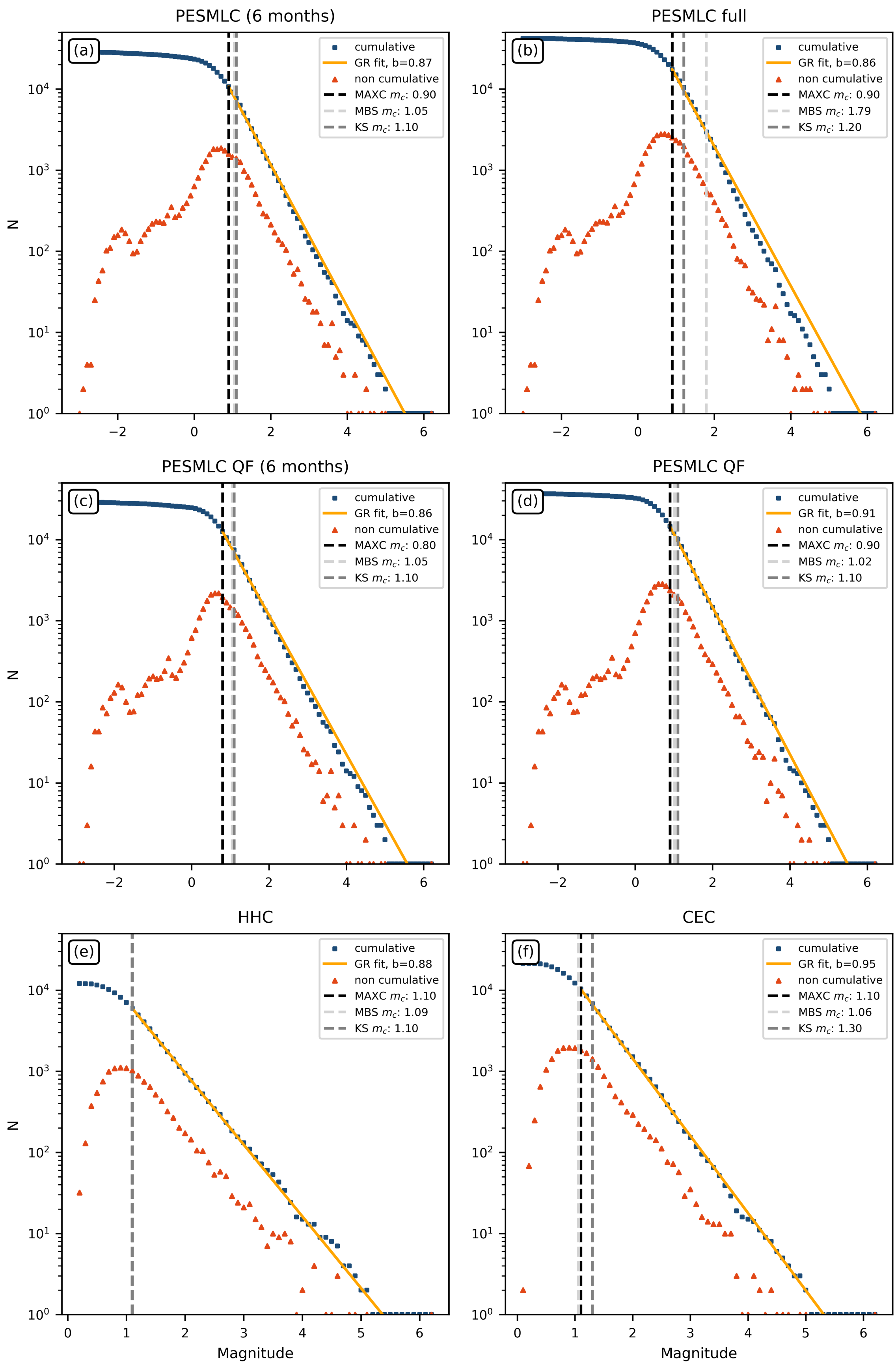

Figure 9 Magnitude of completeness (M_c) and b-value analysis for all three catalogues. Cumulative number of events is plotted in blue and number of events per magnitude bin is plotted in red. Vertical dashed lines indicate M_c estimates from the Maximum Curvature (MAXC, black), b-value stability (MBS, light grey), and Kolmogorov-Smirnov (K-S, dark grey) methods. Top row shows results for the complete PESMLC for the first six months of the sequence (a) and for the full study period (b). Middle row shows results for the quality-filtered PESMLC (QF) for the first six months (c) and for the full study period (d). Bottom row shows results for HHC over the first six months (e) and for CEC over the full study period (f)

				Sliding window			MLE			
Catalogue	Region / duration	M_c	N	K	c (days)	p	t_{cut} (days)	K	c (days)	p
HHC spatial extent, first 6 months										
HHC	HHC / 6 months	1.95	933	118.98	0.057	0.931	0.19	99.8	0.000	0.919
PESMLC	HHC / 6 months	1.95	1061	139.94	0.048	0.971	0.19	120.3	0.000	0.965
PESMLC filtered	HHC / 6 months	1.95	1072	141.40	0.046	0.964	0.20	120.4	0.000	0.959
CEC	HHC / 6 months	1.95	1176	169.40	0.084	0.981	0.30	143.9	0.007	0.972
PESMLC†	HHC / 6 months	1.10	6529	1523.00	0.450	1.093	0.30	1147.1	0.188	1.068
PESMLC filtered†	HHC / 6 months	1.10	6514	1482.26	0.450	1.072	0.30	1092.5	0.157	1.047
Full study region, full duration										
CEC	Full / full	1.95	1497	158.83	0.063	0.937	0.25	135.3	0.000	0.929
PESMLC	Full / full	1.10	11115	909.77	0.105	0.802	0.10	700.5	0.000	0.797
PESMLC filtered	Full / full	1.10	8939	1112.71	0.246	0.932	0.23	816.5	0.000	0.908

Table 2 Omori–Utsu law parameter estimates for all catalogue and method combinations. Sliding window (SW) fits use a window of 15 earthquakes with a 5 earthquake shift, with rates fitted in log-space following Herak and Herak (2023). MLE fits follow (Ogata, 1983) on unbinned event times; t_{cut} is the post-mainshock incompleteness cutoff determined by the parameter sensitivity analysis (see Supplementary Material). Rows marked † are not reported as reliable estimates due to non-convergence of c within the tested parameter range, where c remained non-zero across all tested t_{cut} values when fitting at $M_c = 1.1$. N denotes the number of events used in each fit.

where $n(t)$ is the aftershock rate at time t after the mainshock, K is a productivity parameter, c is a characteristic time offset, and p governs the rate of decay. Herak and Herak (2023) analysed the aftershock decay of the Petrinja sequence using events with $M_L \geq 1.95$ from HHC, applying a sliding window of 15 consecutive earthquakes shifted by 5 events, with the resulting rates fitted in log-space, and reported $p = 0.92$. We extend this analysis in two ways. First, we reproduce and validate their approach across all four catalogues (HHC, PESMLC, quality-filtered PESMLC, and CEC) using the same method, magnitude threshold, and time window. Second, we apply maximum likelihood estimation (MLE) following Ogata (1983), which operates on unbinned event times and provides a more statistically rigorous parameter estimation than least-squares fitting to windowed rates. The post-mainshock incompleteness cutoff t_{cut} is determined objectively for each catalogue via a parameter sensitivity analysis described in the Supplementary Material. Results for all catalogue and method combinations are summarised in Table 2.

Comparison with HHC. Applying the sliding window log-space method to HHC at $M_c = 1.95$ over the first six months of the sequence gives $p = 0.931$, consistent with the published value of 0.92 (Herak and Herak, 2023). MLE on the same catalogue and completeness threshold gives $p = 0.919$, a difference of 0.012, indicating that the choice of fitting method introduces only a small systematic offset at this magnitude threshold. Across all four catalogues, the sliding window method consistently obtains a slightly higher p than MLE (by 0.009–0.030), reflecting the greater weight the sliding window approach assigns to later data points through log-space fitting.

Comparing catalogues at the same $M_c = 1.95$ and 6-month window, PESMLC and CEC obtain higher p values than HHC by 0.04–0.05 (MLE: $p = 0.965$, 0.959, and 0.972 for PESMLC complete, filtered, and CEC respectively, vs $p = 0.919$ for HHC). We attribute this difference to the conservative nature of HHC, which was compiled by a single experienced analyst who deliberately excluded events of uncertain location (Herak and Herak, 2023). The additional events in PESMLC and CEC above $M_c = 1.95$ are predominantly concentrated in the early post-mainshock period, steepening the apparent decay rate and increasing the inferred p. The near-identical results for PESMLC complete and filtered at $M_c = 1.95$ (0.965 vs 0.959) confirm that quality filtering has negligible effect at this high magnitude threshold where the fraction of low-quality detections is small.

Full duration and optimal completeness threshold. Extending the analysis to the full study duration and region, and applying the optimal completeness threshold of $M_c = 1.1$ identified from the sensitivity analysis, reveals a pronounced effect of event quality on the inferred decay exponent. For the complete PESMLC, MLE gives $p = 0.797$ ($t_{\mathrm{cut}} = 0.10$ days, $c = 0$), whereas the quality-filtered PESMLC gives $p = 0.908$ ($t_{\mathrm{cut}} = 0.23$ days, $c = 0$). This difference of $\Delta p = 0.111$ directly demonstrates that low-quality detections in the complete catalogue bias the inferred decay exponent downward, analogous to their effect on M_c estimates discussed in Section 5.4. The longer incompleteness window required for the filtered catalogue ($t_{\mathrm{cut}} = 0.23$ vs 0.10 days) reflects the disproportionate removal of early post-mainshock detections by quality filtering, as low-quality events are most prevalent immediately after the mainshock when waveform overlap and coda interference are most severe.

Notably, the filtered PESMLC result of $p = 0.908$ is in close agreement with the HHC and CEC results at $M_c = 1.95$ (0.919 and 0.929 respectively), despite using a lower completeness threshold and a richer catalogue. This consistency across different catalogues, magnitude thresholds, and time windows suggests that $p \approx 0.91$ represents a robust estimate of the true decay exponent for the Petrinja sequence. The CEC result over the full duration ($p = 0.929$) being nearly identical to the 6-month result ($p = 0.972$ sliding window, $p = 0.929$ MLE at full duration) further confirms that the decay rate is stable across the two-year study period with no evidence of accelerated or slowed aftershock activity after the first six months.

In all reliable fits — those where the sensitivity analysis confirms $c = 0$ — the time offset collapses to zero, indicating no detectable delay in the onset of Omori decay once catalogue incompleteness is properly accounted for. This is consistent with the view that non-zero c values in unconstrained Omori fits are artifacts of post-mainshock catalogue incompleteness rather than a physical feature of aftershock sequences (Utsu et al., 1995). We note that the full study region includes a distal cluster of residual aftershocks from the March 2020 M_w 5.3 Zagreb earthquake (cluster IV in Figure 3), which is a separate fault system. However, given the 9-month interval between the Zagreb mainshock and the start of the Petrinja sequence, the contribution of Zagreb aftershocks to the observed decay rate is expected to be negligible, particularly at $M_c = 1.1$ where the Petrinja aftershock rate dominates throughout the study period.

5.6 Processing time

Finally, the main advantage of the ML approach is the significant reduction in time required to produce seismic catalogues. While the manual approach typically takes several months of dedicated picking and reviewing, our final version of the ML-based catalogue covering the entire study period of 22 months was completed in approximately 3 days. For instance, processing 6 months of seismic data for a single station took roughly 15 minutes, using a batch size of 4,096 on a 16 GB NVIDIA RTX 4060 GPU. This remarkable acceleration enables seismological observatories, particularly those understaffed, to efficiently and accurately generate (preliminary) catalogues, allowing analysts to focus exclusively on manually verifying events above a specific magnitude and quality threshold.

6 Conclusions

The use of machine learning for seismic phase picking and earthquake catalogue creation in the 2020 M_w 6.4 Petrinja earthquake sequence has demonstrated both the potential and challenges of automated approaches. The deployment of EQTransformer, combined with phase association and location using PyOcto and NonLinLoc SSST respectively, allowed us to construct a comprehensive seismic catalogue — Petrinja Earthquake Sequence Machine Learning Catalogue (PESMLC) — that successfully captures the temporal and spatial characteristics of the seismic sequence. PESMLC contains 41,989 events and exhibits excellent matching rates with existing manual catalogues, achieving 96% match rate with the catalogue by Herak and Herak (2023) and an 85% match rate with the Croatian Earthquake Catalogue. Our catalogue detects about two times more events than manual catalogues, identifying previously undetected (micro)seismic events, significantly enhancing our understanding of the seismicity associated with the Petrinja fault zone. However, our analysis also highlights specific limitations inherent to automated methods, particularly event detection challenges for closely timed seismic events. Missed events predominantly occurred due to the inflexible phase association criteria or overlapping seismic phases, underscoring the necessity of training machine learning models on datasets containing overlapping events. The effect of network density on detection capabilities was clearly illustrated by the deployment of temporary networks (OP-Net and PM-Net), which led to a notable improvement in location precision, microseismicity detection, and missed-event reduction.

We also show a counter-intuitive result for magnitude of completeness, where, when using either the b-value stability method or the Kolmogorov-Smirnov method, our ML-generated catalogue has higher values for M_c than manual ones. However, we demonstrate that this effect is driven by low-quality detections rather than genuine network incompleteness. When applied to a quality-filtered subset of PESMLC, the three methods converge to values comparable to or lower than those of the manual catalogues, demonstrating that quality filtering is essential prior to completeness assessment of ML-derived catalogues. Extending the analysis to aftershock temporal decay, we demonstrate that the quality-filtered PESMLC obtains $p = 0.908$, consistent with manual catalogue estimates across different completeness thresholds and time windows, while the unfiltered catalogue gives $p = 0.797$, directly showing that the low-quality detections push the inferred decay exponent downward by a comparable magnitude to their effect on M_c estimates

Beyond the Petrinja sequence itself, this study highlights three broader implications for ML-based seismic monitoring. First, the performance of ML approaches is fundamentally constrained by network geometry, as no algorithm can fully compensate for insufficient station coverage; consequently, the expected source distribution should be considered explicitly during network design. Second, large ML-generated catalogues require quality filtering prior to both completeness assessment and aftershock decay analysis, as low-quality detections cause stricter M_c estimators to produce artificially high completeness thresholds and simultaneously bias Omori decay exponents (p) downward — two effects that, left uncorrected, can have important implications for b-value estimates and aftershock forecasting. Third, the observation that the two manual reference catalogues agree on only 75% of events during their overlapping period emphasises the limitations of treating any single manual catalogue as definitive ground truth, suggesting that multi-catalogue validation approaches are preferable when possible. Collectively, these findings indicate that reliable automated seismic monitoring depends not only on advances in ML algorithms, but also on optimised network design and robust validation strategies. Overall, our results strongly support the integration of ML methods into routine seismic monitoring, as it provides a rapid, detailed, and comprehensive seismic catalogue essential for seismic hazard assessment and mitigation strategies. However, it must be used as a tool, rather than as a replacement for human analysts. Future work is needed and can be focused on refining association parameters in the context of specific regional seismic characteristics and network configurations. Future network geometry planning should also take into account our results — the distribution of sources and the possible weight each station location could have in providing accurate seismic catalogue.

Acknowledgements

This work has been supported by the Norwegian Financial Mechanism 2014-2021 under the project "Investigation of seismically vulnerable areas in Croatia and seismic ground motion assessment – CRONOS", 04-UBS-U-0002/22-90. We would like to thank Marijan Herak for providing us with the catalogue from Herak and Herak (2023) and its phase arrival times and the Croatian Seismological Survey (CSS) for providing us with the seismicity data within the Croatian Earthquake Catalogue (CEC). The authors thank two anonymous reviewers for their comments and suggestions which improved the quality and clarity of this manuscript. We dedicate this work to Jean-Baptiste Ammirati, who contributed to the initial phase of this work and left this world too suddenly.

Data and code availability

The Petrinja Earthquake Sequence Machine Learning Catalogue (PESMLC), matched events between PESMLC and both of the manual catalogues, and codes used in this study are made permanently available at
https://doi.org/10.5281/zenodo.15640710
HHC is available in the Supplementary Material of Herak and Herak (2023).
CEC is available upon request to the Croatian Seismic Survey.
Seisbench, used for phase picking is available from https://github.com/seisbench/seisbench .
Pyocto, used for phase association is available from https://github.com/yetinam/pyocto .
NonLinLoc software can be downloaded from http://alomax.free.fr/nlloc/
HypoDD software can be downloaded from https://www.ldeo.columbia.edu/ felixw/hypoDD.html

Competing interests

G. Hetényi is an editor in Seismica and has fully withdrawn himself from the review process.

References

Allen, R. V. Automatic earthquake recognition and timing from single traces. *Bulletin of the Seismological Society of America*, 68(5): 1521–1532, 1978. doi: 10.1785/bssa0680051521.

Baize, S., Amoroso, S., Belić, N., Benedetti, L., Boncio, P., Budić, M., Cinti, F., Henriquet, M., Jamšek Rupnik, P., Kordić, B., et al. Environmental effects and seismogenic source characterization of the December 2020 earthquake sequence near Petrinja, Croatia. *Geophysical Journal International*, 230(2):1394–1418, 2022.

Basili, R., Kastelic, V., Demircioglu, M., Garcia Moreno, D., Nemser, E. S., Petricca, P., Sboras, S. P., Besana-Ostman, G. M., Cabral, J., Camelbeeck, T., Caputo, R., Danciu, L., Domac, H., Fonseca, J., García-Mayordomo, J., Giardini, D., Glavatovic, B., Gulen, L., Ince, Y., Pavlides, S., Sesetyan, K., Tarabusi, G., Tiberti, M. M., Utkucu, M., Valensise, G., Vanneste, K., Vilanova, S., and Wössner, J. The European Database of Seismogenic Faults (EDSF) compiled in the framework of the Project SHARE, 2013.

Basili, R., Danciu, L., Carafa, M. M. C., Kastelic, V., Maesano, F. E., Tiberti, M. M., Vallone, R., Gracia, E., Sesetyan, K., Atanackov, J., Sket-Motnikar, B., Zupančič, P., Vanneste, K., and Vilanova, S. Insights on the European Fault-Source Model (EFSM20) as input to the 2020 update of the European Seismic Hazard Model (ESHM20), 2020. doi: 10.5194/egusphere-egu2020-7008.

Becker, D., McBrearty, I. W., Beroza, G. C., and Martínez-Garzón, P. Performance of AI-Based Phase Picking and Event Association Methods after the Large 2023 Mw 7.8 and 7.6 Türkiye Doublet. *Bulletin of the Seismological Society of America*, 114(5): 2457–2473, 2024. doi: 10.1785/0120240017.

Cao, A. and Gao, S. S. Temporal variation of seismic <i>b</i> -values beneath northeastern Japan island arc. *Geophysical Research Letters*, 29(9), 2002. doi: 10.1029/2001gl013775.

Cianetti, S., Bruni, R., Gaviano, S., Keir, D., Piccinini, D., Saccorotti, G., and Giunchi, C. Comparison of Deep Learning Techniques for the Investigation of a Seismic Sequence: An Application to the 2019, Mw 4.5 Mugello (Italy) Earthquake. *Journal of Geophysical Research: Solid Earth*, 126(12), 2021. doi: 10.1029/2021jb023405.

Clauset, A., Shalizi, C. R., and Newman, M. E. J. Power-Law Distributions in Empirical Data. *SIAM Review*, 51(4):661–703, 2009. doi: 10.1137/070710111.

Dasović, I., Herak, M., Herak, D., Latečki, H., Sečanj, M., Tomljenović, B., Cvijić-Amulić, S., and Stipčević, J. The Berkovići (BIH) ML= 6.0 earthquake sequence of 22 April 2022–Seismological and seismotectonic analyses. *Tectonophysics*, 875:230253, 2024.

Fonzetti, R., Govoni, A., De Gori, P., Valoroso, L., and Chiarabba, C. Machine learning-based high-resolution data set for the 2009 L'Aquila earthquake sequence. *Geophysical Journal International*, 243(1), 2025. doi: 10.1093/gji/ggaf286.

Herak, D. and Herak, M. The Kupa Valley (Croatia) Earthquake of 8 October 1909–100 Years Later. *Seismological Research Letters*, 81(1):30–36, 2010. doi: 10.1785/gssrl.81.1.30.

Herak, M. Conversion between the local magnitude (ML) and the moment magnitude (Mw) for earthquakes in the Croatian Earthquake Catalogue. *Geofizika*, 37(2):197–211, 2020. doi: 10.15233/gfz.2020.37.10.

Herak, M. Croatian catalogue and database of focal mechanism solutions, characteristic mechanisms, and stress field properties in the Dinarides and the surrounding regions. *Geofizika*, 41 (2):79–123, 2025. doi: 10.15233/gfz.2024.41.5.

Herak, M. and Herak, D. Properties of the Petrinja (Croatia) earthquake sequence of 2020–2021 – Results of seismological research for the first six months of activity. *Tectonophysics*, 858: 229885, 2023. doi: 10.1016/j.tecto.2023.229885.

Herak, M., Herak, D., and Markušić, S. Revision of the earthquake catalogue and seismicity of Croatia, 1908–1992. *Terra Nova*, 8 (1):86–94, 1996. doi: 10.1111/j.1365-3121.1996.tb00728.x.

Herak, M., Herak, D., and Orlić, N. Properties of the Zagreb 22 March 2020 earthquake sequence–analyses of the full year of aftershock recording. *Geofizika*, 38(2):93–116, 2022. doi: 10.15233/gfz.2021.38.6.

Jiang, C., Fang, L., Fan, L., and Li, B. Comparison of the earthquake detection abilities of PhaseNet and EQTransformer with the Yangbi and Maduo earthquakes. *Earthquake Science*, 34(5): 425–435, 2021. doi: 10.29382/eqs-2021-0038.

Kim, A., Nakamura, Y., and Yukutake, Y. Development of high-performance seismic phase picker using deep learning in Hakone Volcanic Area. *Research Square*, 2022. doi: 10.21203/rs.3.rs-2253946/v1.

Lomax, A. and Savvaidis, A. High-precision earthquake location using source-specific station terms and inter-event waveform similarity. *ESS Open Archive*, 2021. doi: 10.1002/essoar.10507108.2.

Lomax, A., Virieux, J., Volant, P., and Berge-Thierry, C. *Probabilistic earthquake location in 3D and layered models: Introduction of a Metropolis-Gibbs method and comparison with linear locations*, page 101–134. Springer Netherlands, 2000. doi: 10.1007/978-94-015-9536-0_5.

Majstorović, J., Giffard-Roisin, S., and Poli, P. Interpreting convolutional neural network decision for earthquake detection with feature map visualization, backward optimization and layer-wise relevance propagation methods. *Geophysical Journal International*, 232(2):923–939, 2022. doi: 10.1093/gji/ggac369.

Markušić, S., Stanko, D., Penava, D., Ivančić, I., Bjelotomić Oršulić, O., Korbar, T., and Sarhosis, V. Destructive M6.2 Petrinja Earthquake (Croatia) in 2020—Preliminary Multidisciplinary Research. *Remote Sensing*, 13(6):1095, 2021. doi: 10.3390/rs13061095.

Michelini, A., Cianetti, S., Gaviano, S., Giunchi, C., Jozinović, D., and Lauciani, V. INSTANCE – the Italian seismic dataset for machine learning. *Earth System Science Data*, 13(12):5509–5544, 2021. doi: 10.5194/essd-13-5509-2021.

Mirwald, A., Schmid, N., Mizrahi, L., Han, M., Rohnacher, A., Ritz, V. A., and Wiemer, S. SeismoStats: a Python package for statistical seismology. *Seismological Research Letters*, 2026. doi: 10.1785/0220250266.

Mizrahi, L., Nandan, S., and Wiemer, S. The Effect of Declustering on the Size Distribution of Mainshocks. *Seismological Research Letters*, 92(4):2333–2342, 2021. doi: 10.1785/0220200231.

Mohorovičić, A. Potres od 8/X 1909.(Das Beben vom 8. X. 1909). *Jahrbuch des meteorologischen Observatoriums in Zagreb (Agram) für das Jahr*, 1909:1, 1910.

Mohorovičić, A. Earthquake of 8 october 1909. *Geofizika*, 9(1):3–55, 1992.

Mousavi, S. M., Ellsworth, W. L., Zhu, W., Chuang, L. Y., and Beroza, G. C. Earthquake transformer—an attentive deep-learning model for simultaneous earthquake detection and phase picking. *Nature Communications*, 11(1), 2020. doi: 10.1038/s41467-020-17591-w.

Münchmeyer, J. PyOcto: A high-throughput seismic phase associator. *Seismica*, 3(1), 2024. doi: 10.26443/seismica.v3i1.1130.

Niksejel, A. and Zhang, M. OBSTransformer: a deep-learning seismic phase picker for OBS data using automated labelling and transfer learning. *Geophysical Journal International*, 237(1): 485–505, 2024. doi: 10.1093/gji/ggae049.

Ogata, Y. Estimation of the parameters in the modified Omori formula for aftershock frequencies by the maximum likelihood procedure. *Journal of Physics of the Earth*, 31(2):115–124, 1983. doi: 10.4294/jpe1952.31.115.

Pita-Sllim, O., Chamberlain, C. J., Townend, J., and Warren-Smith, E. Parametric Testing of EQTransformer's Performance against a High-Quality, Manually Picked Catalog for Reliable and Accurate Seismic Phase Picking. *The Seismic Record*, 3(4):332–341, 2023. doi: 10.1785/0320230024.

Ross, Z. E., Meier, M., Hauksson, E., and Heaton, T. H. Generalized Seismic Phase Detection with Deep Learning. *Bulletin of the Seismological Society of America*, 108(5A):2894–2901, 2018. doi: 10.1785/0120180080.

Ross, Z. E., Yue, Y., Meier, M., Hauksson, E., and Heaton, T. H. PhaseLink: A Deep Learning Approach to Seismic Phase Association. *Journal of Geophysical Research: Solid Earth*, 124(1): 856–869, 2019. doi: 10.1029/2018jb016674.

Sardeli, E., Michas, G., Pavlou, K., Zaccagnino, D., and Vallianatos, F. Spatiotemporal properties of the 2020–2021 Petrinja (Croatia) earthquake sequence. *Journal of Seismology*, 28(4), 2024. doi: 10.1007/s10950-024-10228-1.

Stipčević, J., Poggi, V., Herak, M., Parolai, S., Herak, D., Dasović, I., Bertoni, M., Barnaba, C., and Pesaresi, D. First results from temporary deployment of small seismic network following the Mw=6.4 Petrinja earthquake. In *EGU General Assembly 2021*, online, 2021. doi: 10.5194/egusphere-egu21-16579. 19–30 Apr 2021, EGU21-16579.

Suarez, E., Domínguez-Cerdeña, I., Villaseñor, A., Aparicio, S. S.-M., del Fresno, C., and García-Cañada, L. Unveiling the pre-eruptive seismic series of the La Palma 2021 eruption: Insights through a fully automated analysis. *Journal of Volcanology and Geothermal Research*, 444:107946, 2023. doi: 10.1016/j.jvolgeores.2023.107946.

Sugan, M., Peruzza, L., Romano, M. A., Guidarelli, M., Moratto, L., Sandron, D., Plasencia Linares, M. P., and Romanelli, M. Machine learning versus manual earthquake location workflow: testing LOC-FLOW on an unusually productive microseismic sequence in northeastern Italy. *Geomatics, Natural Hazards and Risk*, 14 (1), 2023. doi: 10.1080/19475705.2023.2284120.

Tan, Y. J., Waldhauser, F., Ellsworth, W. L., Zhang, M., Zhu, W., Michele, M., Chiaraluce, L., Beroza, G. C., and Segou, M. Machine-learning-based high-resolution earthquake catalog reveals how complex fault structures were activated during the 2016–2017 central Italy sequence. *The Seismic Record*, 1(1): 11–19, 2021. doi: 10.1785/0320210001.

Tomac, I., Vlahovic, I., Parlov, J., Matoš, B., Matešic, D., Kosovic, I., Pavicic, I., Frangen, T., Terzic, J., Pavelic, D., et al. Geotechnical Reconnaissance and Engineering Effects of the December 29, 2020, M6. 4 Petrinja, Croatia Earthquake, and Associated Seismic Sequence. Technical report, Technical report of Geotechnical Extreme Event Reconnaissance (GEER ..., 2021.

University of Zagreb. Croatian Seismograph Network, 2001. doi: 10.7914/SN/CR.

Utsu, T., Ogata, Y., S, R., and Matsu'ura. The centenary of the Omori formula for a decay law of aftershock activity. *Journal of Physics of the Earth*, 43(1):1–33, 1995. doi: 10.4294/jpe1952.43.1.

Waldhauser, F. and Ellsworth, W. L. A double-difference earthquake location algorithm: Method and application to the northern Hayward fault, California. *Bulletin of the seismological society of America*, 90(6):1353–1368, 2000.

Wiemer, S. and Wyss, M. Minimum Magnitude of Completeness in Earthquake Catalogs: Examples from Alaska, the Western United States, and Japan. *Bulletin of the Seismological Society of America*, 90(4):859–869, 2000. doi: 10.1785/0119990114.

Woessner, J. and Wiemer, S. Assessing the Quality of Earthquake Catalogues: Estimating the Magnitude of Completeness and Its Uncertainty. *Bulletin of the Seismological Society of America*, 95 (2):684–698, 2005. doi: 10.1785/0120040007.

Woollam, J., Rietbrock, A., Bueno, A., and De Angelis, S. Convolutional Neural Network for Seismic Phase Classification, Performance Demonstration over a Local Seismic Network. *Seismological Research Letters*, 90(2A):491–502, 2019. doi: 10.1785/0220180312.

Woollam, J., Münchmeyer, J., Tilmann, F., Rietbrock, A., Lange, D., Bornstein, T., Diehl, T., Giunchi, C., Haslinger, F., Jozinović, D., et al. SeisBench—A toolbox for machine learning in seismology. *Seismological Society of America*, 93(3):1695–1709, 2022.

Xiong, W., Yu, P., Chen, W., Liu, G., Zhao, B., Nie, Z., and Qiao, X. The 2020<i>M</i>w 6.4 Petrinja earthquake: a dextral event with large coseismic slip highlights a complex fault system in northwestern Croatia. *Geophysical Journal International*, 228 (3):1935–1945, 2021. doi: 10.1093/gji/ggab440.

Zhou, J., Pham, T.-S., and Tkalčić, H. Deep-learning phase-onset picker for deep Earth seismology: PKIKP waves. *ESS Open Archive*, 2024(0422), 2024. doi: 10.22541/essoar.171378807.79679078/v1.

Zhu, W. and Beroza, G. C. PhaseNet: a deep-neural-network-based seismic arrival-time picking method. *Geophysical Journal International*, 2018. doi: 10.1093/gji/ggy423.

Žilić, I., Causse, M., Vallée, M., and Markušić, S. High Stress Drop and Slow Rupture During the 2020 MW6.4 Intraplate Petrinja Earthquake, Croatia. *ESS Open Archive*, 2025. doi: 10.22541/essoar.173724184.40120513/v1.